PCCP

Accepted Manuscript

ROYAL SOCIETY OF CHEMISTRY

www.rsc.org/pccp

The influence of liquid Pb-Bi on the anti-corrosion behaviors of Fe_3O_4: a first-principles study

Dongdong Li[1], Bingyan Qu[1], H. Y. He[2], Y. G. Zhang[3], Yichun Xu[3], B. C. Pan[2*], and Rulong Zhou[1*]

[1] *Laboratory of amorphous materials, School of Materials Science and Engineering, Hefei University of Technology, Hefei, Anhui 230009, P. R. China*

[2] *Hefei National Laboratory for Physical Sciences at Microscale, and Department of Physics, University of Science and Technology of China, Hefei, Anhui 230026, People's Republic of China*

[3] *Key Laboratory of Materials Physics, Institute of Solid State Physics, Chinese Academy of Sciences, P. O. Box 1129, Hefei 230031, P. R. China*

*bcpan@ustc.edu.cn, *rlzhou@hfut.edu.cn

Abstract

In this work, the influence of Pb and Bi atoms on the anti-corrosion behaviors of the oxide film (Fe_3O_4) formed on the steel surface is investigated based on first-principles calculations. Through calculations of the formation energies, we find that Pb and Bi atoms can promote the formation of point defects, such as interstitial atoms and vacancies in Fe_3O_4. Besides, the effects of concentration of Pb (or Bi) and pressure on formation of these defects are also studied. Our results depict that high density of Pb (or Bi) and compression pressure can promote the formation of defects in Fe_3O_4 significantly. Furthermore, the energy barriers for Pb and Bi atoms migration in Fe_3O_4 are also estimated using climbing image nudge elastic band (CI-NEB) method, which implies that Pb and Bi can diffuse more easily in Fe_3O_4 comparing to Fe. Our results reveal the underlying mechanism of how Pb and Bi influence on the anti-corrosion ability of oxide films in accelerate driven system (ADS). It is

instructive for improving the corrosion resistance of the oxide films in ADS.

KEYWORDS

LBE, Fe_3O_4, Vacancies, Interstitial atoms, Pressure, Diffusion

1. Introduction

Lead-Bismuth Eutectic (LBE) is one of the most promising core coolants and target materials in accelerate driven system (ADS) because of their good properties such as low melting point, high boiling point, and high chemical stability when exposed to the gas and water.[1] One of the critical issues associated with the applications of LBE is that usually it may corrode the structural materials (they are usually steels) encapsulating it dramatically because the atoms in the structural materials have high solubility in the liquid LBE.[2, 3] So, the compatibility of the structural materials and LBE has attracted extensive attentions in the past years.[1, 2, 4-15] Large amount of experiments have been performed to probe the anti-corrosion properties of various materials under different working temperatures and exposure times. For example, the anti-corrosion properties of T91 and 316L at the temperatures from 450°C to 560°C were extensively studied.[7, 12, 16-19] Besides, the dissolution corrosion of iron surface exposed to liquid LBE and Lead-Gold Eutectic(LGE) were studied by Xu et al, and the conclusion that Bi atoms have larger corrosion capability than Pb and Au on iron surface were drawn.[10]

On the other way, one may introduce a protective film between the structural materials and LBE to prevent the corrosion. A common method is to dissolve a proper concentration of oxygen into LBE.[2] With oxygen in LBE, a protective oxide film will be formed on the surface of steel and the film will separate the structural materials from LBE. As a result, the dissolution corrosion of LBE will be greatly reduced. The ideal protective film should be pore-free, crack free, and stress free in the operating environment.[13] According to previous works, the oxide films formed on martensitic

steels in LBE have a double-layer structure.[17, 20-22] The inner layer is composed of Fe-Cr spine and the out layer is composed of magnetite (Fe_3O_4). The inner layer grows at the Fe-Cr spinel/steel interface and the out layer grows at magnetite/LBE interface. However, when the temperature is above 550 °C, the protectiveness of the oxide layer formed on the austenitic stainless steels often disappears in corrosion test for long-time exposing,[12, 23-25] whose reason is not very clear. Therefore, it is important to investigate the interactions between the oxide film and LBE. Yeliseyeva et al. reported that the concentration of Pb in the oxide film on the surface of T91 steel will arrive up to 7.63 at.% when it is exposed to oxygen-saturated Pb-Bi melt at 560 °C.[12] The penetration of Pb or Bi into Fe_3O_4 may be the reason for the decrease of the protectiveness of the oxide layer. Sahu et al. have studied the phase diagram of Pb-Fe-O system, which is important to understand the composition and the stability of the oxide film.[26] However, the influence of Pb and Bi on the anti-corrosion properties of Fe_3O_4, especially for the long-term run, is not clear yet, because the studies on the penetration of Pb and Bi atoms into the oxides film at atomic scale are absent from our best knowledge. Literature reported some first-row transition metal such as Mn and Ni can suppress the formation of Fe vacancies in iron(II) oxide.[27, 28] Whether Pb and Bi will suppress or facility the formation of vacancies in Fe_3O_4 is unknown.

In this paper, we perform first-principles calculations to investigate the influences of Pb and Bi on the anti-corrosion behaviors of Fe_3O_4. The favorite sites for Pb and Bi atoms doped in Fe_3O_4 and the effects of Pb and Bi atoms on the formation energy of vacancy and interstitial of Fe atoms in Fe_3O_4 are studied. The results show that the doped Pb and Bi atoms will promote the formation of those defects. The effects of the concentration of Pb and Bi, and that of the pressure on the vacancy formation energies are also studied. Our results show that high density of Pb or Bi and compression pressure can promote the formation of vacancy defects significantly. In addition, the migration of Pb and Bi atoms in Fe_3O_4 are also investigated. The evaluated migration barriers shows that Pb and Bi atoms are easier to migrate in Fe_3O_4 comparing to Fe.

2. Method

The structure relaxations and the total energy calculations are performed within the framework of DFT as implemented in the Vienna *ab initio* simulation package (VASP).[29, 30] The Perdew-Burke-Ernzerhof (PBE) functional within the generalized gradient approximation (GGA) is adopted for exchange-correlation potential.[31] The energy cutoff of the electronic wave functions is 400 eV. A dense k-point sampling with the 4×4×4 k-point mesh in the Brillouin zone is taken. We apply a Hubbard U correction with U=4.5 eV and exchange parameter of J=0.89eV to describe the Fe 3*d* states while not for O, Pb and Bi atoms.[32] Fe_3O_4 possesses the inverse spinel structure containing 24 Fe atoms and 32 O atoms in the conventional cell. The calculated cell parameter is 8.402 Å and it fits the experiment value (8.394 Å) well.[33] For geometry optimization, the lattice parameters and the atomic coordinates are fully relaxed, until the maximum force acting on each atom is lower than 0.02 eV/Å. The transition pathways of Pb, Bi and Fe atoms between different equivalent sites in Fe_3O_4 are studied by using climbing image nudged elastic band (CI-NEB) method,[34, 35] where five images are inserted into the reaction path. In Fe_3O_4, four inequivalent sites including two substitution sites and two interstitial sites are considered, which are tetrahedral sites (A-site), octahedral sites (B-site), octahedral interstitial sites (C-site) and tetrahedral interstitial sites (D-site), as shown in Fig. 1. The doping of Pb and Bi at all the sites (denoted as Pb_A, Pb_B, Bi_A, Bi_B etc) and its influence on the formation of Fe vacancies at A-site or B-site (denoted as V^{Fe}_A and V^{Fe}_B, respectively) and interstitial Fe atoms at C- and D-site (denoted as Fe_C and Fe_D) are considered.

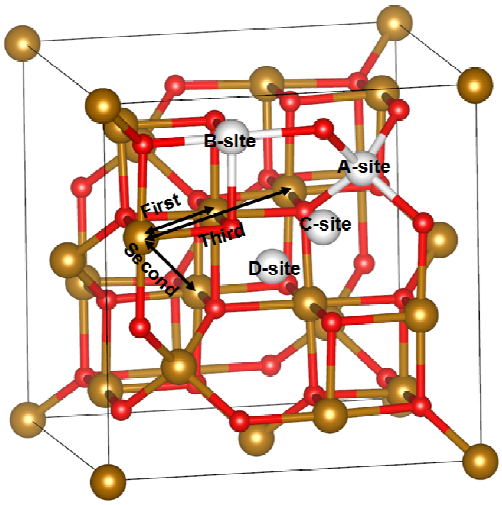

Fig. 1 The structure of Fe_3O_4. Red and brown balls represent O and Fe atoms, respectively. White balls represent different sites in Fe_3O_4. The different neighbors of Fe atoms at B-site are also shown.

3. Results and discussions

3.1 The stability of Pb and Bi doped Fe_3O_4

Usually, Fe_3O_4 is formed at the interface between the steel and LBE at the temperatures higher than 400K, so Pb and Bi atoms may ineluctably enter into the Fe_3O_4 lattice. Firstly, we calculate the formation energy of a Pb (or Bi) atom doping in Fe_3O_4 to determine which site it will be located. Both the substitution sites (A-site or B-site, see Fig. 1) and the interstitial sites (C-site or D-site) are considered. The formation energy of the substitution doping and interstitial doping can be achieved according to formula (1) and (2) respectively:

$$E_f^s = (E_{MFe_{23}O_{32}} - \mu_M) - (E_{Fe_{24}O_{32}} - \mu_{Fe}) \qquad (1)$$

$$E_f^i = E_{MFe_{24}O_{32}} - \mu_M - E_{Fe_{24}O_{32}} \qquad (2)$$

where $E_{Fe_{24}O_{32}}$, $E_{MFe_{23}O_{32}}$ and $E_{MFe_{24}O_{32}}$ are the total energies of perfect Fe_3O_4, substitutionally-doped Fe_3O_4 with M (=Pb or Bi) atom and interstitially-doped Fe_3O_4 with M atom, respectively. μ_{Fe} and μ_M are the chemical potential of Fe and M atoms, respectively. μ_{Fe} is the cohesive energy (energy per atom) of body-centered cubic Fe, while μ_M is the average energy per atom of Pb (or Bi) in LBE.[36]

The calculated formation energies of Pb and Bi doped at all the sites considered

are listed in Table I. Apparently, for the substitutional-doping of Pb and Bi, A-site (Pb_A and Bi_A) is more favored. While for the interstitial-doping, C-site is more favored for Pb and Bi (Pb_C and Bi_C). The optimized structures can be obtained from the supplement materials. However, the formations of interstitial Pb and Bi defects are much more difficult than the formation of interstitial Fe because of almost two times higher formation energies of them comparing to that of interstitial Fe (0.805 eV for Fe_C as listed in Table II).

Because the LBE works at high temperatures up to several hundreds of degrees, the relative stabilities of different phases should be considered. For this purpose, we calculate the Helmholtz free energy F according to

$$F(V,T) = E_0(V) + F_{vib}(V,T) + F_{el}(V,T), \qquad (3)$$

where $E_0(V)$, $F_{vib}(V,T)$ and $F_{el}(V,T)$ are the total energy of the crystal at 0 K, the contributions from ionic vibrational motion and electron thermodynamic motion, respectively. The value of $F_{el}(V,T)$ is very smaller than that of $F_{vib}(V,T)$, so the former can be neglected. In the quasiharmonic approximation, $F_{vib}(V,T)$ can be defined as:

$$F_{vib}(V,T) = \frac{1}{2}\sum_{q\lambda}\hbar\omega_{q\lambda}(V) + k_B T\sum_{q\lambda}\ln\left[1-\exp\left(-\frac{\hbar\omega_{q\lambda}(V)}{k_B T}\right)\right], \qquad (4)$$

where the phonon frequencies are calculated by using VASP combined with Phonopy software.[37] The Helmholtz free energies of Fe_3O_4 with the doping of Pb_A and Pb_B are compared in Fig. 2. Obviously, the free energy of the structure with Pb_A is always lower than that of Pb_B in the whole temperature range, which means that the relative stability of the two phases are not changed in the range of considered temperatures. According to our calculations, the difference between the vibrational free energy of Fe_3O_4 with Pb_A and Pb_B is less than 0.3 eV in the temperature range of 0-1000 K, which is much smaller than that of the total energies at 0 K (0.667 eV). For the other cases, the vibrational free energy difference should be similar to that of Pb doping, because the cells considered are almost the same except the dopants. As listed in Table

I to Table III, the relative formation energies of each defect at different sites are usually much larger than 0.3 eV, so the temperature effect cannot change the relative orders of them.

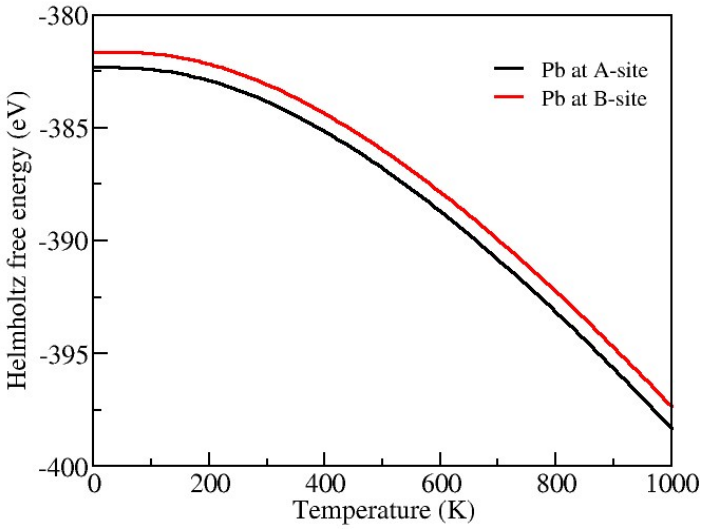

Fig. 2 The Helmholtz free energies of Fe_3O_4 with the doping of Pb_A and Pb_B.

The doping of Pb (or Bi) has a little influence on the magnetic moments of Fe nearby. Usually, Fe_3O_4 is ferrimagnetic, where magnetic moments of Fe_B atoms aligned anti-parallelly with respect to that of the Fe_A atoms at low temperature. In the perfect Fe_3O_4, the Fe atoms at A-site and B-site possess average magnetic moments of -4.02 μ_B and 3.89 μ_B, respectively, and the total moment of the conventional cell is 31.75 μ_B. With the doping of Pb_A (Bi_A), the total magnetic moment of the Fe_3O_4 is increased by 4.0 μ_B (4.8 μ_B), while it is decreased by 5.9 μ_B (4.9 μ_B) with the doping of Pb_B (Bi_B). Particularly, for B-site doping, the direction of the magnetic moments of Fe_B are not changed, but the average magnetic moments of Fe_B closed to Pb_B(Bi_B) is decreased by 0.26 μ_B (0.22 μ_B) compared with that of Fe_B in perfect Fe_3O_4. The average magnetic moments of Fe_A are almost not changed for both A-site doping and B-site doping.

Table I. The formation energies of substitutionally and interstitially doped Pb and Bi in Fe_3O_4.

	Substitution energy E_f^s (eV)		Formation energy of interstitial atom E_f^i (eV)	
	A-site	B-site	C-site	D-site
Pb	1.403	2.070	1.675	2.078
Bi	1.414	2.124	1.668	2.136

Here, only a single Pb or Bi atom contained in the supercell is considered, which approximates the condition of low density of impurities (about 1.5 at.%) in the system. Actually, the concentration of Pb may arise to 7 at.% as mentioned above. So, high density of Pb or Bi impurities in Fe_3O_4 has to be considered too. It is noted that when high density of Pb or Bi atoms penetrating into Fe_3O_4, pseudo binary $(Fe_{1-x}M_x)O$-Fe_2O_3 (M=Pb or Bi) systems may form.[12] Because the doped Pb and Bi atoms are usually distributed randomly in Fe_3O_4, it is hard to reproduce the actual structure. Approximately, we can use special quasirandom structures (SQSs) to represent the random distribution of Pb and Bi atoms in Fe_3O_4.[38, 39] The SQSs configurations are the particular ones which have the highest statistics weight and whose energy can better fit that of the completely random alloy.[40] More details about this method are described in Ref.[38, 39] In our calculations, there are 8 Fe_A atoms and 16 Fe_B atoms in the conventional cell of Fe_3O_4. For simplicity, Pb (Bi) atoms at A-site and B-site are separately treated. Therefore, 8- and 16-atoms/unit cell are respectively used in the SQS model. The restricted cell cannot fully mimic the random alloys and a small difference is expected between the real random alloys and the calculated results. With this method, one fittest configuration of Fe_3O_4 for each concentration of Pb (or Bi) is produced. By using the produced structures, the average substitution energies and the volumetric change rates are calculated, which are shown in Fig. 3. In our calculations, the average substitution energies are defined as

$$\overline{E}_s = [(E_{M_N Fe_{24-N} O_{32}} - N\mu_M) - (E_{Fe_{24}O_{32}} - N\mu_{Fe})]/N, \quad (5)$$

where N is the number of Pb (or Bi) atoms in Fe_3O_4, which ranges from 1 to 7 for B-site and from 1 to 4 for A-site, respectively. The corresponding maximum concentration of Pb (Bi) atoms is 12.5 at.%. From **Error! Reference source not found.**(a), we know that the average substitution energies of Pb at both A-site and B-site decrease monotonously with the increase of the concentration, *i.e.* the more the Pb atoms are in Fe_3O_4, the easier the doping of additional Pb atom is. So, a large concentration of Pb atoms will penetrate into the oxide film in the real sample as found in experiments,[12] which will weaken the anti-corrosion properties of the oxide film. The substitution energies of Pb at A-site are much lower than that at B-site, meaning the substitution of Pb for Fe at A-site is still easier in high concentration cases. With the concentration of 7.143 at.% for Pb, the average substitution energy at A-site is merely 0.9 eV and it is 0.69 eV lower than that at B-site with the same concentration. The situation for Bi doping is similar to that of Pb.

As shown in **Error! Reference source not found.**(b), the volumes of the supercell increase almost linearly as the concentration of Pb and Bi atoms doped in Fe_3O_4. The volumetric change rate of the case of Pb doped at A-sites (Pb_A), Bi doped at both A-sites (Bi_A) and B-sites (Bi_B) are very close, while that of the case of Pb doped at B-sites (Pb_B) are relatively smaller. At the concentration of 7.143 at.% for Pb_A, the volume is about 11% larger than the perfect one. Such large volume change between the Pb or Bi doped and the perfect Fe_3O_4 will make the protecting oxide film wrinkle and easy to be peeled off. Hence, for long-term services, the oxide film will lose its protective ability.

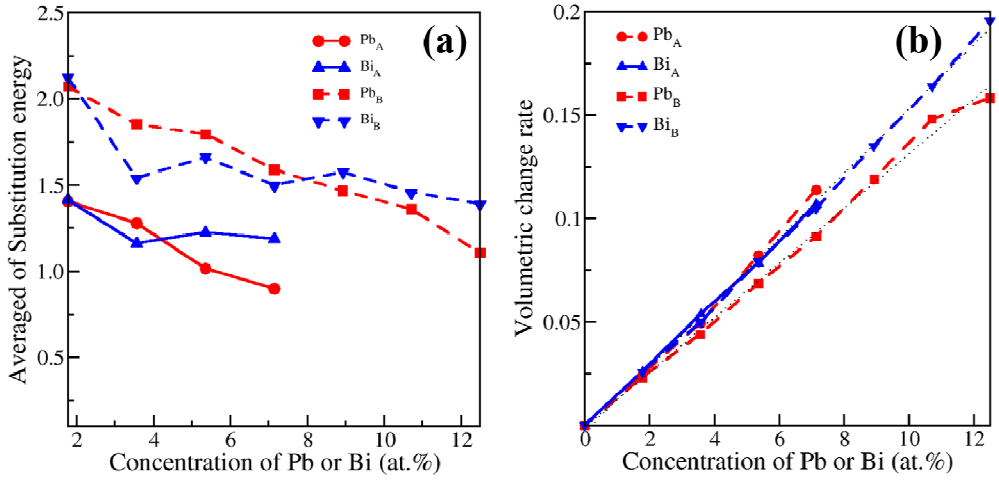

Fig. 3 (a) The average substitution energy and (b) volumetric change rates with respect to the concentration of Pb or Bi atoms in Fe_3O_4, respectively.

3.2 The effects of Pb and Bi on energetics of point defects in Fe_3O_4

Point defects, such as vacancies and interstitial atoms, are inevitably introduced in Fe_3O_4 due to neutron irradiation and thermal excitation in ADS. Usually, the defects will have negative influence on the anti-corrosion behavior of the oxide film formed on the steel surface. Previous experiments have illustrated that pores are often formed in the Fe_3O_4 oxide if the concentration of vacancy is high enough.[41] The pores could break the integrality of oxide film, thus decrease the anti-corrosion capability of the oxide film. As is known, the radii of Pb and Bi ions are much larger than that of Fe, so the doped Pb and Bi ions will not only enlarge the volume of Fe_3O_4, as shown in the above section, but also could induce large internal stress in the lattice of Fe_3O_4. The stress may promote the production and accumulation of point defects. Therefore, it is important to study the influence of the doped Pb and Bi ions on the point defects in Fe_3O_4. Since the formation energies of the defects related with Fe atoms are much lower than those related with O atoms, in this study only the interstitial Fe atoms and Fe vacancies are considered. Based on the formula (2), we firstly calculated the formation energy of an interstitial Fe atom in perfect Fe_3O_4, which are 0.805eV and 1.251eV (see Table I) for C-site interstitial and D-site interstitial, respectively. Then, the formation energies of an interstitial Fe atom in the Pb (or Bi) doped Fe_3O_4 were

calculated by the formula:

$$E_f = E_{MFe_{24}O_{32}} - \mu_{Fe} - E_{MFe_{23}O_{32}}, \qquad (6)$$

where $E_{MFe_{24}O_{32}}$ is the total energy of Fe_3O_4 with a substitutional Pb (or Bi) atom and an interstitial Fe atom inside. The corresponding results are listed in Table II. Both the cases of Pb (or Bi) doped at A-site (Pb_A or Bi_A) and B-site (Pb_B or Bi_B) were considered, and the interstitial sites are close to Pb (or Bi). From Table II, one can see that the induced Pb or Bi atom could largely reduce the formation energies of the interstitial Fe atom at C-site or D-site (Fe_C or Fe_D), except for the case of the Fe_D+Bi_A where the formation energy of Fe_D is almost equal to that in perfect Fe_3O_4. For the Pb_B and Bi_B doped systems, Fe_D cannot locate at D-site stably and it will move to the place close to C-site after structural relaxation. Specially, for Pb_B and Bi_B doped systems, the formation energy of a Fe_C atom nearby is negative, which means that the Fe_C atom tends to form at the neighbor of a Pb_B (or Bi_B) atom. These results strongly indicate that Pb and Bi doping in Fe_3O_4 could largely promote the formation of the interstitial Fe atoms.

Table II. The formation energies of Fe interstitial atoms in perfect and Pb (or Bi) doped Fe_3O_4.

Doped atom	Formation energy of interstitial Fe atom(eV)	
	Fe_C	Fe_D
Without doping	0.805	1.251
Pb_A	0.380	0.765
Pb_B	-0.430	Unstable (0.418)
Bi_A	0.426	1.256
Bi_B	-0.465	Unstable (0.157)

Then, the influences of Pb (or Bi) atoms on the formation of Fe vacancies at A-site or B-site (V^{Fe}_A or V^{Fe}_B) in Fe_3O_4 are studied. The formation energies are calculated according to the formula:

$$E_f = E_{MFe_{22}O_{32}} + \mu_{Fe} - E_{MFe_{23}O_{32}}, \qquad (7)$$

where $E_{MFe_{23}O_{32}}$ and $E_{MFe_{22}O_{32}}$ are the total energy of Fe_3O_4 with an M (M=Pb or Bi) inside and the total energy of Fe_3O_4 with a vacancy in the supercell, respectively. For comparison, the formation energies of V^{Fe}_A and V^{Fe}_B in the perfect Fe_3O_4 are calculated firstly, which are 3.450 eV and 2.300 eV, respectively. The formation energies of Fe vacancies in the Pb (or Bi) doped Fe_3O_4 are listed in Table III. Clearly, only when the doped Pb or Bi and the Fe vacancy are locate at the same type of sites, *i.e.* M_A+V^{Fe}_A or M_B+V^{Fe}_B (M represents Pb or Bi), the decrease of the formation energy of a Fe vacancy is significant. And, the decrement is related with the distance between the Fe vacancy and Pb (or Bi) atom. When they are the nearest-neighboring (1NN), the formation energy of a Fe vacancy can be reduced by 0.4 eV because of the influence of Pb (or Bi). Therefore, Fe vacancies have a trend to gather around the Pb or Bi atoms.

When a vacancy at A-site (B-site) presents in Fe_3O_4, the total magnetic moments will be increased (decreased) by 7.6 μ_B (2.1 μ_B), accordingly. Great increasing of the magnetic moment is observed for the oxygen atoms closed to the vacancy at A-site (about 0.4 μ_B). When the vacancy occupies a B-site, the average magnetic moment of the Fe_B atom closed to V_B is increased by 0.23 μ_B.

Table III. The formation energies of V^{Fe}_A and V^{Fe}_B in the Pb (or Bi) doped Fe_3O_4. M denotes Pb or Bi atoms.

Cases		E_f (eV)	
		Pb	Bi
M_A+V^{Fe}_A		3.163	3.274
M_A+V^{Fe}_B		2.306	2.289
M_B+V^{Fe}_A		3.465	3.325
	1NN	1.998	1.963

$M_B+V^{Fe}_B$	2NN	2.023	2.173
	3NN	2.253	2.233

As mentioned above, the concentration of Pb (or Bi) in LBE may be as large as 7 at.%, where the doped Pb (or Bi) atoms may be very close to each other. The influence of the density of the doped atoms on the formation of Fe interstitial defects and Fe vacancies should be considered. So, the influences of two or three Pb_B (or Bi_B) atoms doped in the same supercell on the formation energies of the interstitial Fe and Fe vacancy in Fe_3O_4 are also studied. With two Pb_B (or Bi_B) atoms in Fe_3O_4, the formation energy of Fe_C nearby is -0.891eV (-0.508 eV), which is obviously lower than the cases with single Pb (or Bi) atom doping. And, the formation energies of V_B are 1.70 eV (1.84 eV) and 1.46 eV (1.53 eV) when there are two Pb (or Bi) and three Pb (or Bi) atoms doped in Fe_3O_4, respectively, which are also obviously lower than that with single Pb (or Bi) atom doped in Fe_3O_4. This implies that the more Pb and Bi atoms in Fe_3O_4 are, the easier the formation of the defects is. So, as more and more Pb or Bi atoms are injected into the Fe_3O_4 film, more defects will form and the protection of the film will become much weaker.

3.3 The effects of pressure on the formation of Fe vacancy in Fe_3O_4

When the Fe_3O_4 film is practically used in ADS, a high compressive or a tensile pressure is loaded on the Fe_3O_4 film. Such a pressure is originated partly from the doped atoms, such as Pb, Bi and so on, and partly from the high shear stress produced by the flowing liquid Pb-Bi.[1] This pressure can accelerate the dissolution corrosion of structural materials and even trip the oxide off from the steel surface. However, the underlying mechanism of the influence of the pressure is still unclear. It may also due to the formation of defects induced by high pressures. So, here, we studied the influence of pressure on the formation energies of Fe vacancies to make sure whether high pressure can promote defects formation.

In Fe_3O_4, the formation energy of a Fe vacancy under hydrostatic pressure is defined as:

$$E_f(p) = H_{Fe_3O_4+V}(p) - H_{Fe_3O_4}(p) + \mu_{Fe}, \qquad (8)$$

where $H_{Fe_3O_4}$ is the enthalpy of Fe_3O_4 and $H_{Fe_3O_4+V}$ is the enthalpy of Fe_3O_4 with a vacancy in the supercell. p denotes the hydrostatic pressure in Fe_3O_4. In the equation (8), enthalpy H is given by $H(p) = E + pV$. In our calculations, pressures ranging from -12 GPa to 12 GPa are considered. Positive values of p represent compression and negative values represent tension. The definition of the formation energy of Fe vacancy in Pb-doped (or Bi-doped) Fe_3O_4 under hydrostatic pressure is similar to formula (6). The calculated formation energies of V^{Fe}_A and V^{Fe}_B under different pressure are calculated and the results are depicted in Fig. 4(a) and Fig. 4(b), respectively.

The formation energy of a V^{Fe}_A without doping (the black line in Fig. 4(a)) is the largest when the pressure is 0 GPa and decreases when compression and tensile pressure are applied, implying that both compression and tensile pressure could promote the formation of V^{Fe}_A. For the case of V^{Fe}_B (the black line in Fig. 4(b)), the formation energy decreases monotonously with the increase of the value of the pressure, imply that only the compression pressure has the ability to promote the formation of Fe vacancies at B-site. Considering the formation energy of a V^{Fe}_B is much lower than that of a V^{Fe}_A under same pressure, so V^{Fe}_B is more important than that of V^{Fe}_A and the compression pressure is more harmful to the Fe_3O_4 film.

From Fig. 4, we can also see that, for the cases with Pb or Bi atoms occupying A-site, the formation energy of a V^{Fe}_A nearby is not only lower, as discussed above, but also decreases more quickly under compression and tensile pressures comparing to that in the case without doping. The decrease of the formation energies of V^{Fe}_A is more significant when Pb or Bi are doped at A-site comparing to B-site. For the Fe vacancy at B-site, the trend of the formation energy is nearly the same to that without doping, while that is greatly reduced when Pb or Bi are doped at B-sites for all the pressures. Since the formation energy of V^{Fe}_B is still lower than that of V^{Fe}_A, the

compression pressure has more influences on the formation of Fe vacancy. In Fig. 4(b), we should note that the formation energy of V_B is about 1.5 eV at the pressure of 12 GPa. Such a low formation energy implies that there will be a large concentration of Fe vacancies in Fe_3O_4.

To obtain a deep insight into the influence of pressure on the concentration of Fe vacancies, we compared the relative concentrations of vacancies under pressures of 6 GPa and 0 GPa. Since the formation energy of V^{Fe}_B is much lower, only the V^{Fe}_B is considered. The thermodynamic equilibrium concentration of vacancies without doping is given by the formula:

$$n \approx N \exp(-E_f / k_B T), \qquad (9)$$

where N is the concentration of Fe_B atoms in Fe_3O_4, k_B stands for the Boltzmann's constant and T refers to the temperature. By using Eq. (9), the concentration ratio of V^{Fe}_B under pressure of 6GPa and 0GPa is estimated by: $\frac{n_p}{n_0} = \exp\left[-\frac{E_f(p) - E_f(0)}{k_B T}\right]$, where $E_f(p) - E_f(0)$ equals to -0.188 eV. At the temperature of 800K, which is in the range of working temperature of LBE, the calculated ratio of $\frac{n_p}{n_0}$ is 15.3. This means that the equilibrium concentration of V^{Fe}_B will greatly increase with compression pressure in the oxide film. As we know, vacancies are negative to the protective abilities of the oxide film. The increasing concentration of the vacancies caused by the compression pressure has large negative influence on the oxide film.

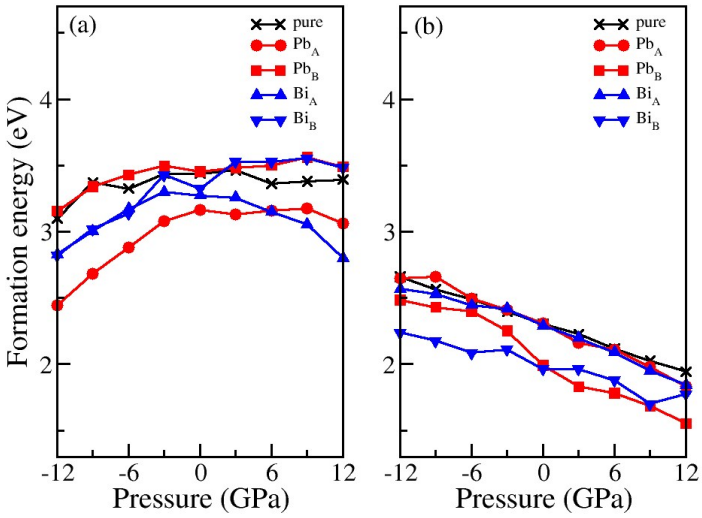

Fig. 4 The formation energy of (a) a V^{Fe}_{A} and (b) a V^{Fe}_{B} as a function of pressure loaded on the Fe_3O_4. The positive values of stress represent the compression pressure and the negative denote the tension pressure.

3.4 The diffusion of Pb and Bi atoms in Fe_3O_4

The migration of Fe atoms in Fe_3O_4 has been studied and it is closely related with the growth and breakdown behavior of the oxide film.[42] The protective oxide film forms on the steel surface and it is directly in contact with liquid Pb-Bi. Pb and Bi atoms will inevitably penetrate into the oxide films and accumulate in them, resulting in promoting the formation of point defects and reducing the anti-corrosion abilities. In this process, the diffusion of Pb and Bi atoms in Fe_3O_4 is very important.

Firstly, the diffusion of Pb and Bi atoms from A-site to C-site are studied. The CI-NEB method is adopted to evaluate the migration barrier of a Pb (or Bi) atom diffusing from A-site to C-site.[34, 35] Previous work has revealed that the energy increase linearly when a Fe atom is moved from A-site to C-site in Fe_3O_4 when A-site is occupied,[42] which means that the interstitial Fe atom at C-site is unstable when one A-site is vacant and the opposite A-site is occupied (C-site is in the center of two closed A-sites). Therefore, in our calculations, the Fe atom at the opposite A-site is removed to make Pb or Bi stay stably at C-site. The calculated energy versus the reaction coordinate is shown in Fig. 5(b). The energy barrier for a Pb (or Bi) atom diffusion is 0.364eV (0.362eV), while that of the reverse process is 0.390eV (0.271 eV). For the diffusion of Fe from A-site to C-site, the calculated migration barrier

using the same method is 0.725 eV and that of the reverse process is 0.598 eV, respectively. Obviously, Pb and Bi atoms are much easier to jump between A-sites sub-lattice in Fe_3O_4 comparing to Fe atoms.

Moreover, the diffusion of a Pb (or Bi) atom from B-site to B-site nearby is also studied and the results are shown in Fig. 5(c) and Fig. 5(d). The corresponding migration barriers for the Pb and Bi atom in Fe_3O_4 are 0.644eV and 1.044 eV respectively, and they are a little higher than that of Fe atom (0.608 eV). This means that Pb and Bi atoms are relatively hard to migrate between B-site sub-lattice in Fe_3O_4. Hence, the diffusion of Pb and Bi atoms in Fe_3O_4 are mainly between A-sites.

When Pb and Bi atoms diffuse through the oxide films and directly interact with the structural materials, dissolution corrosion of the structural materials will be accelerated. For long-term services of the oxide films in liquid Pb-Bi environment, there will be a high concentration of Pb and Bi atoms in it, as a result, the concentration of vacancies will increase accordingly and pores will be produced by the accumulation of vacancies. Besides, with Pb and Bi atoms present in Fe_3O_4, pressure will be introduced and crack will be induced accordingly, thus the anti-corrosion abilities of the oxide film will be decreased.

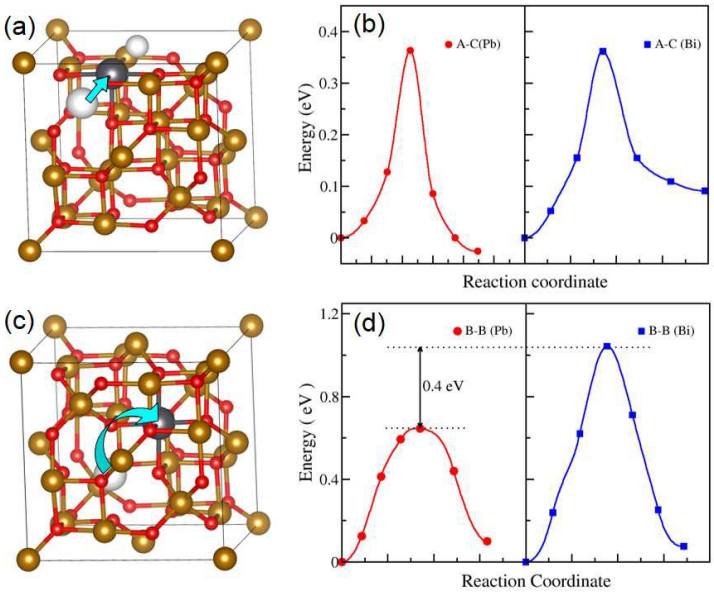

Fig. 5 (a) and (c) are the schematic diagram for the diffusion from A-site to C-site and B-site to B-site

respectively, (b) and (d) are the energy curves of the two diffusion processes respectively.

4. Conclusions

In summary, in this work we systematically study the influence of Pb and Bi on the anti-corrosion ability of Fe_3O_4 based on first-principles calculations. The calculated formation energies indicate that Pb and Bi can easily form in Fe_3O_4. The impurity of Pb and Bi can promote the formation of Fe vacancies and interstitial defects especially at the conditions of high concentration of impurities. Pressures can further lower the formation energies of Fe vacancies. The diffusion of Pb and Bi atoms in Fe_3O_4 are also investigated and the results depict that Pb and Bi atoms are easy to diffuse in the oxide film. All these results indicate that Pb and Bi atoms in LBE can penetrate into the Fe_3O_4 protecting film and promote the formation and accumulation of point defects, so that decrease the anti-corrosion ability of the Fe_3O_4 film gradually. Our results reveal the underlying mechanism of how Pb and Bi influence on the anti-corrosion ability of oxide films in ADS. It will be helpful for finding effect ways to improve the corrosion resistance of the oxide film in ADS.

Acknowledgements

This work is financially supported by the National Magnetic Confinement Fusion Program (Grant No. 2013GB107004), the National Natural Science Foundation of China (No. 11105140, 11275191). The computational center of USTC are acknowledged for computational support.

5. Reference

1. J. Zhang and N. Li, *Journal of Nuclear Materials*, 2008, 373, 351-377.
2. N. Li, *Journal of Nuclear Materials*, 2002, 300, 73-81.
3. J. R. Weeks, *Nuclear Engineering and Design*, 1971, 15, 363-372.

4. Y. Kurata, M. Futakawa and S. Saito, *Journal of Nuclear Materials* 2004, 335, 501-507.
5. M. Kondo and M. Takahashi, *Journal of Nuclear Materials*, 2006, 356, 203-212.
6. A. Doubkovα, F. D. Gabriele, P. Brabec and E. Keilova, *Journal of Nuclear Materials*, 2008, 376, 260-264.
7. A. Jianu, G. Müller, A. Weisenburger, A. Heinzel, C. Fazio, V. G. Markov and A. D. Kashtanov, *Journal of Nuclear Materials*, 2009, 394, 102-108.
8. C. Schroer, A. Skrypnik, O. Wedemeyer and J. Konys, *Corrosion Science*, 2012, 61, 63-71.
9. A. Heinzel, A. Weisenburger and G. Müller, *Journal of Nuclear Materials*, 2014, 448, 163-171.
10. Y. C. Xu, C. Song, Y. Zhang, C. S. Liu, B. C. Pan and Z. G. Wang, *Phys. Chem. Chem. Phys.*, 2014, 16, 16837-16845.
11. G. Müller, A. Heinzel, J. Konys, G. Schumacher, A. Weisenburger, F. Zimmermann, V. Engelko, A. Rusanov and V. Markov, *Journal of Nuclear Materials*, 2004, 335, 163-168.
12. O. Yeliseyeva, V. Tsisar and G. Benamati, *Corrosion Science*, 2008, 50, 1672-1683.
13. J. Zhang, *Corrosion Science*, 2009, 51, 1207-1227.
14. Y. Kurata, *Journal of Nuclear Materials*, 2014, 448, 239-249.
15. Y. E. Zhang, Y. W. You, D. D. Li, Y. C. Xu, C. S. Liu, B. C. Pan and Z. G. Wang, *PCCP*, 2015, 17, 12292-12298.
16. Y. Kurata, H. Yokota and T. Suzuki, *Journal of Nuclear Materials*, 2012, 424, 237-246.
17. L. Martinelli, F. Balbaud-Célérier, A. Terlain, S. Delpech, G. Santarini, J. Favergeon, G. Moulin, M. Tabarant and G. Picard, *Corrosion Science*, 2008, 50, 2523-2536.
18. C. Schroer, O. Wedemeyer, A. Skrypnik, J. Novotny and J. Konys, *Journal of Nuclear Materials*, 2012, 431, 105-112.
19. C. Schroer and J. Konys, *Journal of Engineering for Gas Turbines and Power*, 2010, 132, 082901.
20. L. Soler, F. J. Martín, F. Hernández and D. Gómez-Briceño, *Journal of Nuclear Materials*, 2004, 335, 174-179.
21. G. Benamati, C. Fazio, H. Piankova and A. Rusanov, *Journal of Nuclear Materials*, 2002, 301, 23-27.
22. G. Müller, A. Heinzel, J. Konys, G. Schumacher, A. Weisenburger, F. Zimmermann, V. Engelko, A. Rusanov and V. Markov, *Journal of Nuclear Materials*, 2002, 301, 40-46.
23. Y. Kurata, M. Futakawa and S. Saito, *Journal of Nuclear Materials*, 2005, 343, 333-340.
24. Y. Kurata and S. Saito, *Materials transactions*, 2009, 50, 2410-2417.
25. C. Schroer, O. Wedemeyer, J. Novotny, A. Skrypnik and J. Konys, *Journal of Nuclear Materials*, 2011, 418, 8-15.
26. S. K. Sahu, R. Ganesan and T. Gnanasekaran, *Journal of Nuclear Materials*, 2012, 426, 214-222.
27. M. C. Toroker, *The Journal of Physical Chemistry C*, 2014, 118, 23162-23167.
28. M. Toroker and E. Carter, *J Mater Sci*, 2015, 50, 5715-5722.
29. G. Kresse and J. Hafner, *Physical Review B*, 1993, 47, 558-561.
30. G. Kresse and J. Hafner, *Physical Review B*, 1993, 48, 13115-13118.
31. J. P. Perdew, K. Burke and M. Ernzerhof, *Physical Review Letters*, 1996, 77, 3865-3868.
32. H.-T. Jeng, G. Y. Guo and D. J. Huang, *Physical Review Letters*, 2004, 93, 156403.
33. M. Fleet, *Acta Crystallographica Section B: Structural Crystallography and Crystal*

Chemistry, 1981, 37, 917-920.

34. G. Henkelman, B. P. Uberuaga and H. Jo´nsson, *Journal of Chemical Physics*, 2000, 113, 9901-9904.
35. G. Henkelman and H. Jo´nsson, *Journal of Chemical Physics*, 2000, 113, 9978-9985.
36. D. D. Li, C. Song, H. Y. He, C. S. Liu and B. C. Pan, *Phys. Chem. Chem. Phys.*, 2014, 16, 7417-7422.
37. A. Togo and I. Tanaka, *Scripta Mater.*, 2015, 108, 1-5.
38. A. Zunger, S. H. Wei, L. Ferreira and J. Bernard, *Physical Review Letters*, 1990, 65, 353-356.
39. S. H. Wei, L. Ferreira, J. Bernard and A. Zunger, *Physical Review B*, 1990, 42, 9622-9649.
40. U. Tinivella, M. Peressi and A. Baldereschi, *J. Phys.: Condens. Matter*, 1997, 9, 11141-11114.
41. H. Hu, Z. Zhou, M. Li, L. Zhang, M. Wang, S. Li and C. Ge, *Corrosion Science*, 2012, 65, 209-213.
42. S. Hendy, B. Walker, N. Laycock and M. Ryan, *Physical Review B*, 2003, 67, 085407.